Iron-doped natural clays: low-cost inorganic adsorbents for phosphate recovering from simulated urban treated wastewater

Diana Guaya[a,b], Rocío Jiménez[a,c], Janeth Sarango[a,d], César Valderrama[b], José Luis Cortina[b]

[a] Department of Chemistry and Exact Sciences, Universidad Técnica Particular de Loja, Loja, Ecuador

[b] Department of Chemical Engineering, BarcelonaTECH-UPC, Barcelona, Spain

[c] Biomass to Resource Group, Universidad Regional Amazónica Ikiam, Napo, Ecuador

[d] Agroecological area, Instituto Superior Tecnológico Cariamanga, Loja, Ecuador

*Correspondence should be addressed to: Diana Guaya

deguaya@utpl.edu.ec

Abstract

Natural inorganic adsorbents are attractive for pollutants removal due to the easy operation, non-toxic characteristics and low cost. In this study, two raw clays (C_1 and C_2) were doped with iron and evaluated for the recovery of phosphate from simulated urban treated wastewater. The adsorbents performances were evaluated through batch adsorption assays. Iron was stably retained in doped clays (C_1-Fe and C_2-Fe) at basal and edge surface at adsorption and desorption stages. Clay adsorbents were effective for adsorption of phosphate at neutral pH 7 and in broad range of phosphate concentrations. The maximum phosphate adsorption capacity values were 21, 38, 21 and 38 for C_1, C_1-Fe, C_2 and C_2-Fe, respectively. The equilibrium sorption data of raw and iron-doped clays were well described by the Langmuir isotherm model (R^2 > 0.97). Therefore, monolayer phosphate adsorption occurred through hydrogen bonding and complexation between protonated hydroxyl groups and phosphate anions. The raw and iron-doped clay adsorbents reached the equilibrium within 10 minutes and the equilibrium attainment data were well described

by the intraparticular diffusion model (R^2 > 0.96). The phosphate monolayer adsorption was followed by diffusion through the internal clay pores. The phosphate adsorption by clays in presence of competing ion was inhibited by the higher ionic charge of sulphate. Besides, the less hydrated chloride and bicarbonate anions promoted the reduction of the sorption capacity of phosphate. Finally, the reusability of iron-doped clays is limited. Therefore, saturated iron-doped clays as single-use adsorbents can be disposed for soil amendment applications.

Keyword: iron hydroxides; phosphate recovery; low-cost-sorbent; sustainable use of resources

1. Introduction

Sources of natural phosphorous sources are limited worldwide, and their high demand predicts a shortage in the coming years. At the industrial level, phosphorus is used for the manufacture of fertilisers, as well as other applications such as cleaning products, food and beverages, and metallurgy. The phosphorus from detergents and household wastes is the largest inorganic source of phosphate-phosphorous forms in natural water bodies and in domestic wastewater. Anthropogenic phosphorus from agricultural runoff, farming waste, industrial and domestic sewage is discharge into the aquatic bodies and is then responsible for eutrophication [1]. Furthermore, the massive increase in the use of cleaning products due to the pandemic makes the short-term eutrophication scenario even worse.

A recent study on phosphorus-flow analysis demonstrated that wastewater treatment plants (WWTP) are considered as the most important secondary source of phosphorus (more than 40%) [2]. Therefore, the removal of phosphate from wastewater containing nutrients is important to conserve the natural aquatic environment [3] and even more important is the recovery of phosphorous from WWTP. Its recovery would also reduce the dependence on external supplies of phosphate rock by recovering it within the phosphorous cycle.

Several processes such as precipitation with Fe(III) salts and crystallisation as struvite with Mg(II) salts from the richest streams (e.g., sewage sludge anaerobic digestion side-streams) are used for this purpose [4]. However, the high operating costs limit the large deployment of these technologies in medium and small-sized WWTPs [5]. The low levels of phosphate in wastewater according to the current regulatory framework make current technological solutions too expensive, so it is necessary to propose effective and low-cost technological strategies. Ion exchange and adsorption are postulated as viable option to recover phosphate forms from both, the total phosphorous-richest side streams and more diluted main streams with total phosphorous levels below 5 mg/L P (16 mg/L P-PO_4^{3-}). The use of several polymeric anion exchangers resins have been reported to be excellent phosphate adsorbents due to its selectivity and sensitivity [6] in streams with low content of dissolved organic matter.

Accordingly, low-cost and environmentally friendly materials are nowadays preferred for the phosphate recovery from wastewater, such as zeolites (clinoptilolite [7], attapulgite [8]), industrial wastes (e.g., fly ash, blast furnace slag, organic/inorganic hybrid adsorbents) [9], and clays (e.g., bentonites, allophane nanoclay) [10]. Clay exhibits a net negative charge, which gives them an important cation adsorption and cation exchange properties. The clay structure and the pH of the aqueous phase determine the development of adsorption and exchange properties of the clays. The use of clays in environmental applications has been reported for the adsorption of toxic pollutants: transition metals, organic micro-pollutants (e.g., biocides and dyes) from wastewater; however, the affinity of clays for phosphate adsorption is very low. The use of hybrid selective phosphate adsorbents such as clays modified by physical and chemical methods is proposed to increase their affinity for oxyanions such as arsenate, selenite and phosphate [11]. The modification protocols based on iron oxide-constructed nanomaterials have reported high stability and potential application [12]. Besides, other metal ions as zirconium(IV) loaded fibrous adsorbent have been reported as efficient phosphate adsorbent [3]. Exceptionally, allophane is a clay type with several

environmental applications due to its interaction with toxic anions. The small particle size, high surface area and aluminol groups at the surface allow a high retention capacity for anions [13].

The development of low-cost material is proposed as a single-use adsorbent, assimilating it as a chemical, for example, as coagulant that could be dosed in the sedimentation or filtration stages in the WWTP. The levels of total phosphorous could reach values from 5 to 15 mg/L P or 50 to 250 mg/L P at main- and side streams, respectively [14]. In the case of countries where more than 80% of the sludge is disposed or applied in agriculture or for soil improvement, such mixtures will improve their fertilising value [15]. Since, phosphate-loaded Fe-adsorbents could function as slow-release fertilisers where the inorganic phosphate could be released under the controlled root mechanism [16].

To the best of our knowledge, several modified clays have been developed for phosphate removal, but we have not found no previous studies that report detailed experimental information about iron-doped clays for phosphate adsorption. The literature review provided of the field indicated that adsorbents rarely develop high phosphate adsorption in neutral pH range [17]. The pH is a critical operational parameter because in a full-scale application the treated wastewater is usually at neutral pH (e.g., 6 to 8.5), therefore it will not require pH adjustment. In this study, iron-doped clays are prepared with the ability to recover phosphate efficiently at neutral pH range values. This work describes the preparation of the iron-doping stage and in batch experimental set-up, the effectiveness and selectivity were evaluated. The specific objectives were: i) to investigate the iron-doping onto raw clays to remove phosphate at neutral pH range, i) to investigate the iron-doping onto raw clays to recover phosphate at neutral values, ii) to study the effect of initial phosphate concentration to determine the clay adsorbent capacity, iii) to study the phosphate adsorption kinetics, iv) to determine the selectivity of clay adsorbents for phosphate adsorption over competing ions and (v) to evaluate the regeneration of clays after phosphate adsorption or their potential application as single-use adsorbent.

2. Materials and Methods

2.1. Clay adsorbent preparation

The raw clay samples were obtained from the San Cayetano formation C_1 sample (3° 56' 41.64" S, 79° 12' 29.16" W, C_1 sample) and from the Zalapa formation C_2 sample (3° 53' 51.72" S, 79° 15' 24.12" W, C_2 sample) from Ecuador. The raw clays were located in the Loja Miocene Sedimentary Basin located at the Central Andes Cordillera in southern Ecuador. The raw clays in bulk were crushed and washed with deionised water and subsequently dried in an oven at 80°C for 24 h. The raw clays were dry sieved to obtain homogeneous adsorbent particle sizes. Particles below 200-µm mesh were used for the experiments. Furthermore, to prepare the iron-doped clay forms (C_1-Fe and C_2-Fe), the clay samples were treated with 0.5 M of $FeSO_4$ solution. A mass:volume ratio of 25 g:250 mL of clay sample and iron sulphate solution, respectively was used. The mixture was stirred under reflux conditions (at 95 ± 2°C) for 4 hours. The pH (7) of the mixture was maintained by the constant addition of a 0.1 M NaOH solution. Then, the treated clays were recovered from the mixture, the iron-doping procedure was repeated twice under the same conditions. Finally, the resulting iron-doped clays were repeatedly washed and centrifugated with deionised water, until not chloride ion was detected in the discharge. The resulting material was vacuum-filtered and dried in an oven at 90 ºC for 24 h. The C_1-Fe and C_2-Fe doped clay samples were stored in a desiccator for further characterization and for adsorption experiments.

2.2. Clays physicochemical characterisation

The sample structures were characterised by a powder X-ray Diffractometer. X-ray diffraction (XRD) patterns were acquired on a powder X-ray Diffractometer (D8 Advance A25 Bruker) with a Cu Kα anode (λ = 0.1542 nm) operating at 40 kV and 40 mA. The diffraction patterns were collected at 25°C and over an angular range from 4 to 60° of 2θ by a fast lineal LynxEyeXE detector. Nitrogen

gas adsorption method was used to determine the specific surface area of the adsorbents with an automatic adsorption analyser using the multipoint Brunauer–Emmett–Teller (BET) method. The morphology of clay samples was studied by a field emission scanning electron microscope (FE-SEM). In addition, a wavelength dispersive X-ray fluorescence spectrometer (Bruker S1 Turbo SD-LE Mining Calibrations) was used to determine the composition of the sample. The infrared absorption spectra were recorded with a Fourier Transform FTIR spectrometer in the range of 4000–550 cm^{-1}. KBr was used to prepare a table sample, and the spectra were obtained by collecting 32 scans using a 4 cm^{-1} resolution. Clay adsorbents were equilibrated with solutions at different ionic strengths to determine the point of zero charge (PZC) by the pH drift method in the range of pH 3–10 as described in a previous work [18]. The test was replicated four times for each sample and the average data is reported.

2.3. Phosphate batch adsorption studies

The phosphate adsorption by raw and iron-doped clays was evaluated under optimal conditions obtained in our previous works and which are summarized in **Error! Reference source not found.**. The phosphate solutions used in the adsorption tests were prepared by dissolving $NaH_2PO_4.2H_2O$ stock solution (1000 mg/L) in deionised water. The pH of the phosphate solutions used in the adsorption test were adjusted using 0.1 M HCl or 0.1 M NaOH. After, phosphate solution-clay adsorbent system was equilibrated it was centrifuged at 5000 rpm and the supernatant filtered (0.45 µm) before analysis. The pH of the initial and final solution was measured using a combined glass electrode (CrisonTM) at room temperature (22 ± 2°C). In the phosphate solution, the pH values were adjusted with an accuracy greater than 0.02 units. The potenciometer calibration was carried out with standard buffer solutions of pH 2, pH 4 and pH 7. The concentration of the initial and equilibrated phosphate solutions were measured using the standard methods for the examination of water and wastewater. A calibration curve was prepared from the phosphate stock solution by using the vanadomolybdophosphoric acid colourimetric method (4500-P C). [19], using

149 a wavelength 470 nm. Cation and anion concentrations including iron ion were determined using a
150 Thermo Scientific Ionic Chromatograph (Dionex ICS-1100 and ICS-1000). The tests were
151 performed in batch by triplicate, and the average values are reported.
152 The equilibrium adsorption capacity was calculated by Eq. 1.

153 $$Q_e = \frac{V \times (C_o - C_e)}{w} \quad \text{(Eq. 1)}$$

154 where Q_e was the equilibrium adsorption capacity (mg/g PO_4^{3-}), V was the volume of phosphate
155 solution (L), C_0 and C_e were the initial and equilibrium concentration of the phosphate solution
156 (mg/L PO_4^{3-}), and w was the mass of the clay material (g).

157 **2.3.1. Phosphate adsorption as a function of pH**

158 The influence of pH on phosphate adsorption by clay adsorbents was evaluated using phosphate
159 solutions at initial pH values between 3 to 10.

160 **2.3.2. Equilibrium adsorption capacity**

161 The sorption capacity of clays adsorbents was determined using a wide range of initial
162 concentrations 10–2000 mg/L PO_4^{3-} at pH 7 (pH was used adjusted according to the expected
163 treated wastewater conditions). The weighted amounts of raw and modified clays were equilibrated
164 by mixing with the phosphate solution in a rotatory stirrer.
165 The equilibrium adsorption isotherms were fitted to the linearised Langmuir (Eq. 2) and Freundlich
166 (Eq. 3) equations:

167 $$\frac{C_e}{Q_e} = \frac{C_e}{Q_m} + \frac{1}{K_L Q_m} \quad \text{(Eq. 2)}$$

168 $$\ln Q_e = \ln K_F + \frac{1}{n} \ln C_e \quad \text{(Eq. 3)}$$

169 where Q_m is the maximum adsorption capacity (mg/g PO_4^{3-}), K_L Langmuir adsorption constant
170 (L/mg), K_F (mg/g) and n were Freundlich constant.
171 The separation factor R_L was a dimensionless constant that explains the Langmuir isotherm shape.
172 The favourability of the adsorption process is defined when $0 < R_L < 1$ and can be calculated by Eq.
173 4.

$$R_L = \frac{1}{1 + K_L C_0} \quad \text{(Eq. 4)}$$

2.3.3. Effect of competing ions

The clay samples were equilibrated in solutions containing a binary combination of phosphate and the coexisting anions (e.g., nitrate, bicarbonate, chloride and sulphate) at equal concentration level. In addition, the phosphate adsorption phosphate was evaluated considering a combination of all competing anions at same concentration level.

2.3.4. Kinetic of phosphate adsorption

The kinetic behaviour of phosphate adsorption by clay adsorbents were evaluated using two liquid/adsorbent dosages. Samples (5 mL) were withdrawn at given times for determining the phosphate concentrations in solution.

The phosphate adsorption capacity as a function of time was calculated by Eq. 5.

$$Q_t = \frac{V \times (C_o - C_t)}{w} \quad \text{(Eq. 5)}$$

where Q_t was the adsorption capacity as a function of time (mg/g PO_4^{3-}), V is the volume of phosphate solution (L), C_0 and C_t were the initial and concentration of the phosphate solution at specific time (mg/L PO_4^{3-}) and w was the mass of the clay material (g).

The experimental kinetic data were fitted to the Homogeneous Diffusion Model (HDM) and the Shell Progressive Model (SPM) in order to describe the phosphate recovery by clay adsorbent materials. The HDM model considered the clay as a quasi-homogeneous media, and the adsorption diffusion rate is a controlling step on the spherical particles defined by Equations 6 and 7 [20]:

i) if particle diffusion D_p ($m^2\ s^{-1}$) controls the adsorption rate, it is described by Eq. 6:

$$-\ln(1 - X(t)^2) = k_p t = \frac{2\,\pi^2 D_p}{r^2} t \quad \text{(Eq. 6)}$$

ii) if liquid film diffusion D_f ($m^2\ s^{-1}$) controls the adsorption rate, it is described by Eq. 7:

$$-\ln\big(1 - X(t)\big) = k_f t = \frac{D_f C}{h\, r\, C_r} t \quad \text{(Eq. 7)}$$

where X(t) was the fractional attainment of adsorption equilibrium between the solid and liquid phase (q_t/q_e) at time t; C and C_r (mg/L) were the concentrations of solute in a solution and the adsorbent phase, respectively; t was the contact time (min); r is the average radius of clay particles (particles below 200 mesh ≈ particles diameter: 7.4×10^{-5} m or particles radius: 3.7×10^{-5} m) and h was the thickness of film around the clay particle (1×10^{-5} m for a poorly stirred solution) [21]. In the SPM, as the porosity of the clay could be considered small and thus practically impervious to the aqueous solution, the phosphate adsorption process is described by a concentration profile of the solution containing phosphate ions going forward into a spherical partially saturated clay particle [20]. The adsorption rate-controlling steps on the clay particles were defined by:

(a) if it was controlled by the fluid film (K_F (m/s)), described by Eq. 8:

$$X(t) = \frac{3C_{s0}K_F}{a_s r C_c}\, t \qquad \text{(Eq. 8)}$$

(b) if it was controlled by the diffusion through the particle adsorption layer (D_p (m^2/s)), described by Eq. 9:

$$\left[3 - 3(1 - X(t))^{2/3} - 2X(t)\right] = \frac{6D_p C_{s0}}{a_s r^2 C_c}\, t \qquad \text{(Eq. 9)}$$

(c) if it was controlled by the chemical reaction (k_s ((m.mol)/(L.s))), described by Eq. 10:

$$\left[1 - (1 - X(t))^{1/3}\right] = \frac{k_s C_{s0}}{r}\, t \qquad \text{(Eq. 10)}$$

where a_s was the stoichiometric coefficient; and C_c and C_{s0} were the concentration of solute at clay unreacted core and in bulk solution, respectively (mg/L).

2.3.5. Phosphate desorption

The raw and doped clay samples were equilibrated with 100 mg/L PO_4^{3-} solution. The solid samples were separated from the aqueous phase for further tests. Therefore, the loaded clay samples were further equilibrated in closed containers using deionised water at pH 3, 6 and 10.

Table 1 Operating conditions of the phosphate adsorption by raw C_1, C_1-Fe, C_2 and iron-doped C_2-Fe clay adsorbents.

Process factors	Conditions
Initial pH (3, 4, 5, 6, 7, 8, 9, 10)	Temperature = 22°C ± 2°C; agitation= 100 rpm; volume: 25 mL; initial PO_4^{3-} concentration= 25 mg/L; contact time = 60 min
Initial concentration (10, 25, 50, 100, 250, 500, 1000, 2000 mg/L)	Temperature = 22°C ± 2°C; pH= 7; agitation= 100 rpm; volume: 25 mL; sorbent dosage= 0.1 g; contact time = 60 min
Kinetic adsorption (2.5 and 5 g)	Temperature = 22°C ± 2°C; pH= 7; agitation= 100 rpm; volume: 500 mL; sorbent dosage= 0.1 g; initial PO_4^{3-} concentration= 100 mg/L; contact time = 5 seg, 10 seg, 30 seg, 45 seg, 60 seg, 2.5 min, 5 min, 10 min, 15 min, 20 min, 30 min, 40 min, 50 min, 60 min
Competing ions (nitrate, bicarbonate, chloride and sulphate)	Temperature = 22°C ± 2°C; pH= 7; agitation= 100 rpm; volume: 25 mL; sorbent dosage= 0.1 g; initial PO_4^{3-} concentration= 50 mg/L; initial competing ion concentration= 50 mg/L; initial coexisting ions concentration= 50 mg/L; contact time = 5 seg, 10 seg, 30 seg, 45 seg, 60 seg, 2.5 min, 5 min, 10 min, 15 min, 20 min, 30 min, 40 min, 50 min, 60 min
Desorption essays (pH 3, 6, 10)	Temperature = 22°C ± 2°C; pH= 7; agitation= 100 rpm; volume: 25 mL; sorbent dosage= 0.1 g; initial PO_4^{3-} concentration= 100 mg/L: contact time = 60 min
Optimal conditions	Temperature = 22°C ± 2°C; pH= 7; agitation= 100 rpm; volume: 25 mL; sorbent dosage= 0.1 g; initial PO_4^{3-} concentration= 25 mg/L; contact time = 60 min

3. Results and Discussion

3.1. Clay and Fe-doped clay characterisation

The X-ray diffraction patterns of raw and iron-doped clays C_1, C_1-Fe, C_2 and C_2-Fe are depicted in Figure 1. The XRD patterns of raw and iron-doped clays at lower angles (4–10º) and at wide angles (10–60º) are represented. The analysis indicated that the C_1 raw clay was a heterogeneous clay material composed of 65.9% montmorillonite (Mt) [$(Na,Ca)_{0,3}(Al,Mg)_2Si_4O_{10}(OH)_2$], 18.5% anorthite

(At) [$CaAl_2Si_2O_8$] and 15.6% quartz (Qt) (SiO_2). The analysis of C_2 raw clay determined that it was also a heterogeneous clay composed of 25.4 % dickite (Dt) [$Al_2Si_2O_5(OH)_4$], 51.9% illite (It) [$(K,H_3O)(Al, Mg, Fe)_2(Si, Al)_4O_{10}[(OH)_2,(H_2O)]$] and 22.8% quartz (Qt) (SiO_2).

The diffraction patterns of the doped clays did not exhibit the formation of a new crystalline mineralogical phases after iron doping. A decrease of the peak intensities was observed for both iron-doped clays in comparison to parent clays. This effect has been attributed to the lower crystallinity of clays due to the presence of Fe (III) ions [22]. The basal space d_{001} plane was calculated as 15 Å for the raw C_1 clay at 2θ: 5.9, which was comparable to the d_{001} value of the montmorillonite pattern. Montmorillonite is a 2:1 layer clay mineral consisting of one Al^{3+} octahedral sheet between two Si^{4+} tetrahedral sheets. The permanent negative charge on the montmorillonite surface occur by the isomorphous substitution of Al^{3+} for Si^{4+} in the tetrahedral layer and the substitution of Mg^{2+}, Zn^{2+} and Fe^{3+} for Al^{3+} in the octahedral layer. The hydrated cations like Na^+ and Ca^{2+} are in the interlayer space which depends of the water content [23]. The iron-doped clay C_1-Fe d_{001} value was 16.35 Å, which has a slight increase in the basal space as consequence of the change of the interlayer cation nature. A similar behaviour was reported before for an iron activated montmorillonite where the iron polyhydroxy cations promoted a partial exchange of Ca^{2+} and Na^+ interlayer metal ions by Fe^{3+} and K^+ [24]. It was also reported the enlarge of basal space for an iron activated montmorillonite nanocomposite where the interlayer metal ions were replaced by hydrogen ions which are intercalated into the silicate layers and the interlayer water is lost during the modification process [23].

The basal space d_{001} plane was calculated as 9.9 Å for the raw C_2 clay at 2θ: 8.9, which was comparable to the d_{001} value of the illite pattern. Ilite clay is a typical 2:1 cationic layered silicate that consists of one central (Si/Al/Fe/Mg) octahedron bound to two (Si/Al) tetrahedrons with K as the intermediate cation. The iron-doped clay C_2-Fe d_{001} value was 10.9 Å, which was a slight increase in comparison to C_2 raw clay. The enlarge of the basal space of illite clays have been

253 previously reported as consequence of the exchange of K^+ ions by divalent cations (e.g., Ca^{2+},
254 Mg^{2+}) which is an extremely slow mechanism [25]. The potassium from basal surface and edge-
255 interlayer have been recognized as exchangeable with other cations.
256 Since, iron can be found in clays as: i) structural iron, ii) iron complexed by surface hydroxyl groups
257 and iii) iron bound by ion exchange at basal siloxane surfaces and at the edge surface [26]. It is
258 confirmed that iron has been retained in C_1-Fe and C_2-Fe clays at basal and edge surface. The
259 specific surface area of C_1, C_1-Fe, C_2 and C_2-Fe clay samples are detailed in **Error! Reference**
260 **source not found.**. The incorporation of iron also promoted the increase of specific surface up to
261 80% and 90% for C_1-Fe and C_2-Fe, respectively, in comparison to the raw clay. Otherwise, opposite
262 effect about the reduction of surface area of the functionalized amino form (NH_2-SBA-15) in
263 comparison with the parent prepared mesoporous silica material (SBA-15) was reported. There
264 was reported values of surface area up to 170 and 406 m^2/g respectively for SBA-15 and NH2-
265 SBA-15. The decrease of surface area value were reported as effect of the existence of functional
266 groups in both outer surface as well as the mesoporous channels [27]. Also, other mesoporous
267 materials MCM-41 with extremely high surface area of 1450.9 m^2/g, has been reported as excellent
268 adsorbent for wastewater treatment [28]. The existence of a higher adsorbent surface area is
269 associated to a larger variability of reactive sites and then higher adsorption capacities can be
270 obtained [29]. However, the surface area values that have been reported for clay adsorbents in this
271 study are lower than the mesoporous materials ones.

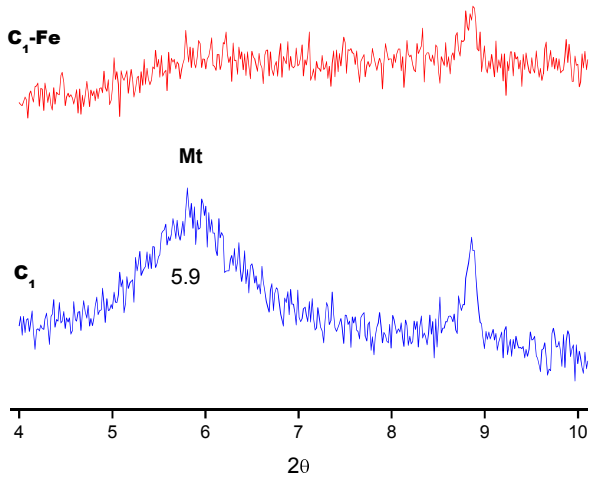

272 a)

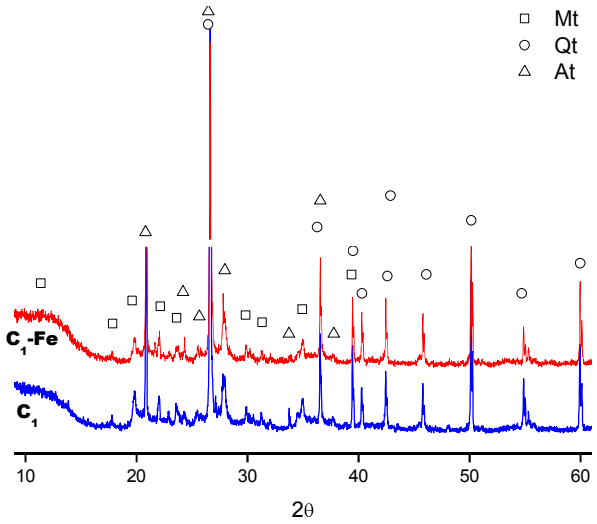

273

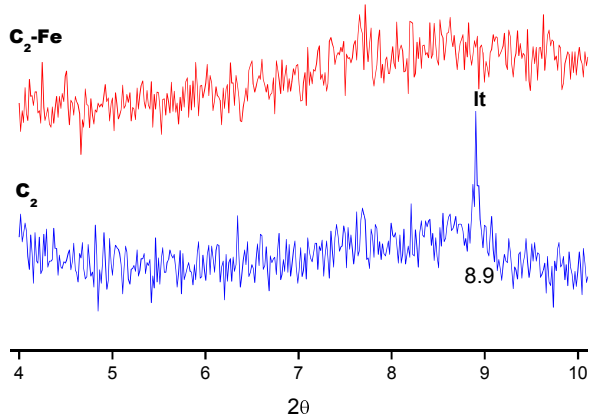

b)

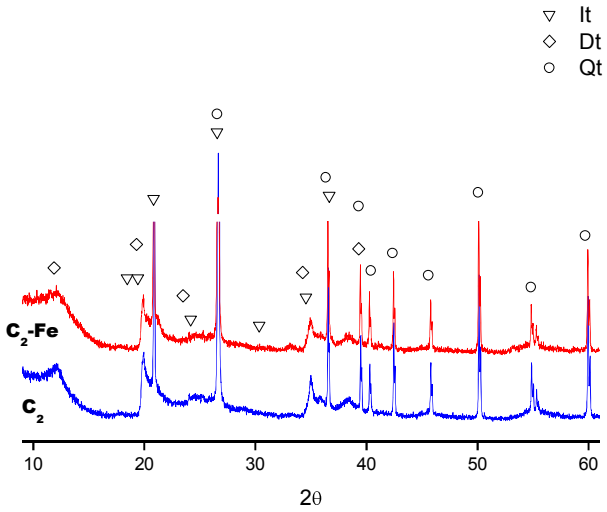

Figure 1 X-ray diffraction patterns of the low and wide angle of a) C_1 and C_1-Fe, b) C_2 and C_2-Fe clay. (Mt: montmorillonite, Qt: quartz, At: anorthite, It; illite, Dt: dickite)

The FSEM analyses of raw clays C_1 and C_2 presented a homogeneous morphology with plate-like crystal surface distribution with a smooth surface (Figure S1 and S2 of the supplementary section). Particularly, in raw clay C_1, there are some rod-like morphology minerals on the surface. A conventional plate-like structure is a representative shape for clays; however, some rod-like structure shapes were previously attributed to some other raw clays. Also, other pedogenic iron

oxide particles were associated with the rod-like morphology [30]. Some changes occurred in the morphology of both iron-doped clays C_1-Fe and C_2-Fe with the appearance of small particles clustered covering the surface. However, the amorphous nature of these iron-hydroxide phases did not allow their identification by XRD analysis. Furthermore, the FSEM-EDX results (data not shown) revealed also the increase of iron on the clay materials used in this study.

The X-ray fluorescence analysis revealed the chemical composition of C_1, C_1-Fe, C_2 and C_2-Fe clay samples and the SiO_2/Al_2O_3 ratio (Table 2). The C_1 and C_2 clays were mainly composed of SiO_2 and Al_2O_3. Other components such as Fe_2O_3, CaO, MgO, Na_2O, K_2O were in low contents for both clays. In addition, raw clays are heterogeneous clays with SiO_2/Al_2O_3 ratios of 5.3 and 2.7 for C_1 and C_2, respectively. The presence of TiO_2 also was determined for clay C_1 at a higher content than in clay C_2. The iron content of both raw clays increased after the modification process. The iron oxide content of C_1-Fe and C_2-Fe clays increased 7% and 20%, respectively, after the iron doping process. The exhausted loading solution of both iron-doped C_1-Fe and C_2-Fe clays was verified by ICP and the release of cations were found (e.g., Mg^{2+}, K^+, Na^+, Ca^{2+}, data not shown). Thus, ion exchange reactions occurred between Fe^{2+}/Fe^{3+} ions with the interchangeable cations (Mg^{2+}, K^+, Na^+, Ca^{2+}) from the raw clays, as described by Eq. 11:

$$\text{Clay-}Mg^{2+} / Na^+ / K^+ / Ca^{2+} + Fe^{2+}/Fe^{3+} \rightarrow \text{Clay-}Fe^{2+}/Fe^{3+} + Mg^{2+} / Na^+ / K^+ / Ca^{2+} \quad \text{(Eq. 11)}$$

The Na content is almost the same for both raw and modified clays. Thus, sodium exchanges again from solution to the iron doped clays while NaOH was added for maintaining the pH. The increase of the pH during iron doping on clays was performed to favour the formation of iron mineral phases in presence of dissolved oxygen. It is worth mentioning that oxidation of Fe(II) to Fe(III) could be favoured at this condition.

Table 2 Chemical composition of C_1, C_1-Fe, C_2 and C_2-Fe clay samples, SiO_2/Al_2O_3 ratio and specific surface area.

Clay materials	Chemical composition[a]								SiO_2/Al_2O_3 ratio	Specific surface area (m^2/g)
	SiO_2	Al_2O_3	Fe_2O_3	CaO	MgO	Na_2O	K_2O	TiO_2		
C_1	74.7	14.2	2.9	1.4	2.8	1.3	2.1	0.6	5.3	28
C_1-Fe	74.8	14.5	3.1	1.3	2.7	1.2	2.0	0.4		50
C_2	68.9	25.1	2.4	1.3	0.3	0.7	1.2	0.1	2.7	28
C_2-Fe	69.1	25.0	2.9	1.1	0.2	0.6	1.1	<lq.[b]		53

[a] Composition of clay samples based on XRF analyses (weight %)

[b] Below of the limit of quantification (<lq). The limit of detection is specified for SiO_2 matrix in three sigma 99.7% confidence level and 120 second analysis time and the error is below 0.5%.

The functional groups present in raw clays C_1 and C_2 were determined (Figure S3, supplementary section). The absorption bands at 3622 cm^{-1} and 3614 cm^{-1} of C_1 and C_2, respectively, were attributed to the external -OH groups. The bands at 3420 and 3693 cm^{-1} for C_1 and 3435 and 3691 cm^{-1} for C_2 were assigned to the internal -OH groups (physisorbed water molecules). These hydroxyl groups can be distinguished by a doublet in these bands [31]. The stretching vibrations of Si-O-Si groups were confirmed in C_1 and C_2 by the presence of the bands at 997 cm^{-1} and 1022 cm^{-1}, respectively. The bending vibration of Al-OH-Si was confirmed in both clays by the appearance of the bands at 768 and 791 cm^{-1} for C_1 and C_2, respectively [32]. In addition, the bands at 2402 and 1651 cm^{-1} for C_1 and at 2380 and 1633 cm^{-1} for C_2 were registered as indicative for the basic layer silicate structures existent on raw and iron-doped clays [33]. There were minimal changes at the wavenumber and positions of the main vibration peaks, which demonstrates that the structural transformation of clays after iron doping did not occur. The variation of the position and the intensity of bands at 1227, 1089 and 793 cm^{-1} for C_1-Fe and the bands at 1228, 1090 and 795 cm^{-1} for C_2-Fe confirms that the Si-O bonds were broken due to partial incorporation of Fe into

the three-dimensional silica network. For Fe-exchanged smectite, the Si-O-Fe bonds were confirmed with the presence of new bands at 634 cm^{-1}, as was obtained in this study for C_1-Fe (688 cm^{-1}) and C_2-Fe (666 cm^{-1}) [33]. The shift of the bands of Si-O-Si groups was at 1028 cm^{-1} for C_1-Fe and 1038 cm^{-1} for C_2-Fe. The shift of the bands of internal–OH groups (for C_1-Fe at 3398 and 3672 cm^{-1} and C_2-Fe at 3398 and 3672 cm^{-1}) and external–OH groups (for C_1-Fe at 3613 cm^{-1} and C_2-Fe at 3622 cm^{-1}) also occurred in iron-doped clays in comparison to raw clays. The -OH group bands were related to the stretching mode of water molecules from the interlayer and clay surface [34]. Thus, the modification of the both iron-doped clays C_1-Fe and C_2-Fe occurred then at these sites forming iron hydroxide bonds. The vibration modes of the iron hydroxide (Fe-O-H) species occurred at 1003 and cm^{-1} for C_1-Fe and 1007 and cm^{-1} C_2-Fe, respectively. However, it may overlap with the conventional vibration mode of clays. Thus, the vibration mode of iron species formed is not well resolved in the infrared spectra [35]. After, the phosphate loading on iron-doped clays, the silicate layer structures were conserved. The loaded phosphate clays C_1-Fe and C_2-Fe presented shifts of the bands of Si-O-Si and iron hydroxide (Fe-O-H) groups, resulting in unique bands at 1009 cm^{-1} and 1001 cm^{-1}, respectively [33].

Considering the characterization of raw and iron-doped clays, iron was retained on C_1-Fe and C_2-Fe in different proportion in accordance with their structure, which determines their reactivity and enable the chemical modification.

3.2. Effect of pH on the adsorption of phosphate

The phosphate adsorption capacities of raw clays C_1 and C_2 were improved after iron particles were incorporated on C_1-Fe and C_2-Fe clays under the evaluated pH conditions. The initial pH of the solution plays an important role in phosphate adsorption (Figure 2). The points of zero charge of the raw clays C_1 and C_2 were found to be 5.2 ± 0.2 and 4.7 ± 0.4, respectively. After being doped, the points of zero charge were 7.2 ± 0.2 and 6.7 ± 0.1 for C_1-Fe and C_2-Fe, respectively. The values of the zero charge points of this study were comparable with those reported for other

clay materials in their raw and iron-doped state [36]. The increase of the point of zero charge values of the doped clay represents a valuable improvement of adsorbent properties due to the existence of iron and iron-(hydr)oxides on the surface. Since hydroxylation occurs when the existing iron on the surface of the clays is exposed to water, which promotes coordination with hydroxyl groups.

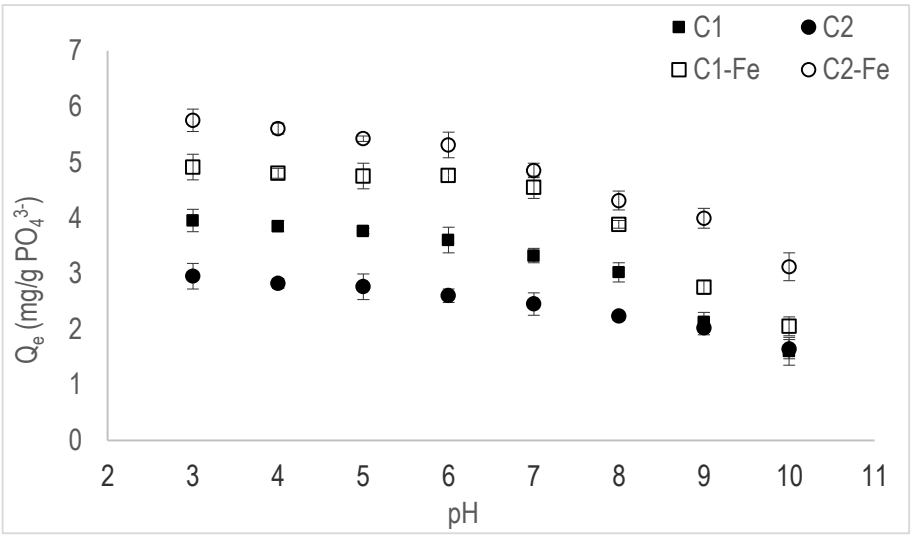

Figure 2 Phosphate adsorption capacity (Q_e (mg/g PO_4^{3-})) removal by raw and doped clays as function of the initial pH solution (V: 25 mL, w: 0.1 g and C_i: 25 mg/L PO_4^{3-}).

The phosphate adsorption capacity exhibited by both raw and iron-doped clays followed the same trend since it increased in the range of pH solutions from 3 to 6 (below pH_{PZC}) and decreased from 7 to 10 (above pH_{PZC}). These results endorsed the oxyanionic speciation of phosphate (H_2PO^{4-} - HPO_4^{2-}), and the pH_{PZC} of the adsorbents played an important role in the adsorption stage. Since clay minerals contains also other surface hydroxyl groups (e.g., AlOH) in its external basal or edge surface. Under pH conditions below the pH_{PZC}, the protonation of iron hydroxyl groups promote positive charges that generate an electric field. The clay adsorbents used in this study in contact with an aqueous medium at this pH condition develop positive charges. Therefore, these sites are very reactive for phosphate interaction through hydrogen bonding interactions. Considering the speciation of phosphate anion in aqueous solutions at the experimental conditions (pH 7), both $H_2PO_4^-$ (ca. 60%) and HPO_4^{2-} (ca. 40%) anionic forms were present. Phosphate anions (HPO_4^{2-})

have high basicity with a pair of high electronic density that can form hydrogen bond with the protonated iron-doped clay surface -$(OH)^+$ [37][38]. At pH conditions above the pH_{PZC}, the hydroxylation occurred and the hard Lewis base (OH^- ions) compete with phosphate oxyanions adsorption (especially HPO_4^{2-}) at the clay surface [39]. The occurrence of physisorption or non-specific phosphate adsorption by electric interactions forces (outer-sphere adsorption complexes) is observed in this study, thus, phosphate is adsorbed by iron oxi(hydroxy) surface groups existent on the surface of raw and doped clays in this study [40]. An advantage of the raw and iron-doped clays used in this study in comparison to many other functional materials, is the effectiveness of phosphate removal at pH between 6 and 7, which is the usual pH condition for surface water and treated wastewater. Therefore, iron-doped clays can be an efficient alternative for the phosphate recovery from wastewater treatment plants at neutral pH of main- or side-streams after anaerobic digestion [17].

3.3. Phosphate adsorption isotherms

The phosphate adsorption capacities of clays in their doped C_1-Fe and C_2-Fe forms were higher than for C_1 and C_2 raw clays (Figure 3 a, b). The increase of phosphate adsorption capacity was around 80% higher in modified clays in comparison to the raw clays. The maximum adsorption capacity of an adsorbent is one of the most important physicochemical parameter to characterize the adsorbent performance [41]. The phosphate equilibrium adsorption capacity as a function of the equilibrium concentration of the four clay samples followed a similar trend. Then, the data provide evidence of the use of iron-doped clays for sensitive phosphate adsorption from a broad range of concentration in treated wastewater. A similar result was reported for a mesoporous silica and ligand embedded composite adsorbent, where higher phosphate concentration provided a driving force that promotes the easier mass transfer from aqueous phase to solid material surface [38]. The Langmuir and Freundlich isotherm were used to identify the phosphate adsorption behaviour by the clay adsorbents (Table 3). The experimental data were best fitted to the Langmuir

isotherm model or monolayer adsorption, thus, indicating that phosphate adsorption takes place at specific equivalent and identical fixed sites [42].

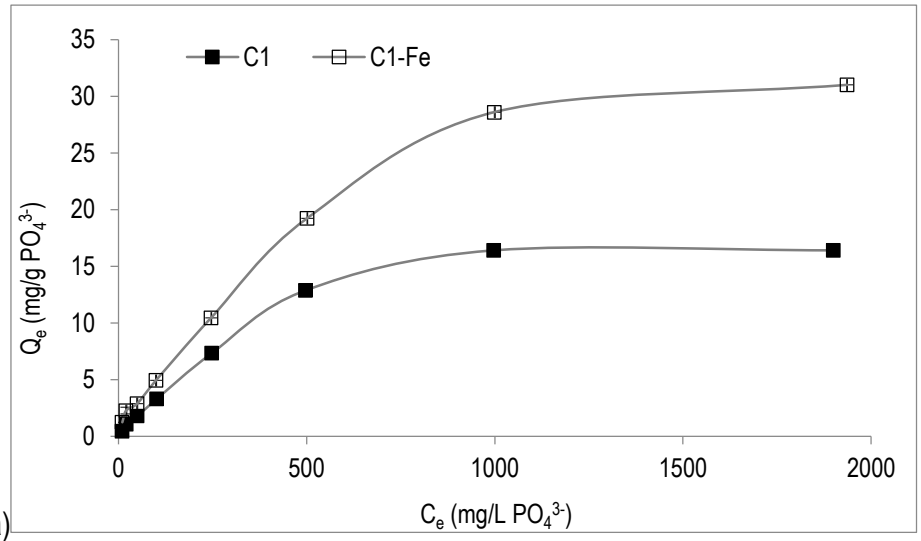

a)

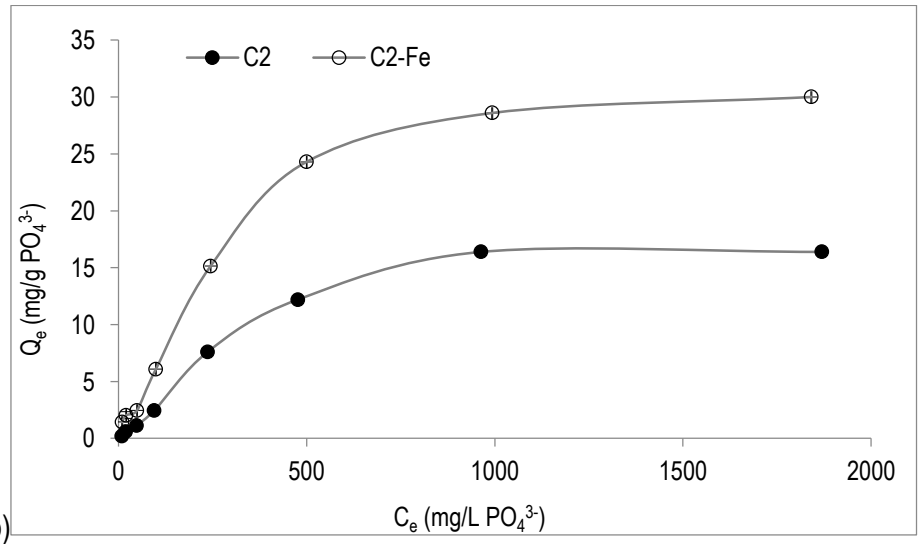

b)

Figure 3 Isotherms of phosphate uptake by clays in raw and Fe-doped forms: a) C_1 and C_1-Fe and b) C_2 and C_2-Fe (V: 25 mL, w:0.1 g and pH: 7)

The highest regression coefficient (R^2) values were obtained for the Langmuir isotherm model for all clays: C_1, C_2, C_1-Fe and C_2-Fe, and the maximum adsorption capacities values determined were 21.4 ± 2.3, 20.9 ± 1.6, 38.0 ± 2.6 and 37.6 ± 3.3 mg/g PO_4^{3-}, respectively. In addition, the separation factor value was determined to be $0 < R_L < 1$ for all clay adsorbents, thus phosphate adsorption by clay adsorbents is favourable. The Freundlich isotherm model represent multilayer

adsorption that occur on heterogenous surface energy active sites [43]. The experimental data fitting revealed the lowest R^2 value for the phosphate adsorption. This fact was expected since clays have a homogeneous morphology and a smooth surface. The examination of phosphate adsorption data using Freundlich isotherm model was discard onto a mesoporous silica and ligand embedded composite adsorbent due to its homogeneous surface [38].

The results suggested the existence of a second mechanism of phosphate adsorption by clays due to specific reactions in both raw and iron-doped forms. The phosphate adsorption onto the raw C_1 and C_2 clays occurred mainly due to the surface hydroxyl groups. The iron incorporated into the C_1-Fe and C_2-Fe clays improved the phosphate adsorption capacity due to the increase of iron surface hydroxyl groups. It is worth mentioning that iron was not detected in the equilibrated solutions. Therefore, the iron complexed by surface hydroxyl groups are chemical stable and highly relevant groups for phosphate removal at the expected pH of treated urban wastewater. Phosphate can replace the protonated hydroxyl groups generated at the clay's surfaces, promoting mono-dentade and bi-dentade complexation process. The protonated hydroxyl groups on the adsorbent surface allowed the phosphate inner sphere complexation reactions. The phosphate can be bounded to an iron atom forming the mononuclear form or phosphate can be bound to two iron to the bidentate form which is schematically described by Eq. 12 [7].

$$
\begin{array}{lll}
 & \mathrm{H_2PO_4^-} \quad pKa = 2.14 \longrightarrow & \mathrm{C-Fe-O-}\overset{\overset{OH}{|}}{\underset{\underset{O}{||}}{P}}\mathrm{-OH} + OH^- \quad Monodentate \\
\mathrm{C-}Fe\mathrm{-OH} + & Complexation\ pH \cong pH_{PZC} & \mathrm{C-Fe} < \begin{matrix} O \\ O \end{matrix} > P \leqslant \begin{matrix} OH \\ O \end{matrix} + OH^- \quad \begin{matrix} Bidentate \\ Mononuclear \end{matrix} \\
 & \mathrm{HPO_4^{2-}} \quad pKa = 7.20 \longrightarrow & \begin{matrix} \mathrm{C-Fe-O} \\ \mathrm{C-Fe-O} \end{matrix} > P \leqslant \begin{matrix} OH \\ O \end{matrix} + 2OH^- \quad \begin{matrix} Bidentate \\ Binuclear \end{matrix}
\end{array}
\qquad \text{(Eq. 12)}
$$

Table 3 Langmuir and Freundlich isotherms parameters obtained for phosphate adsorption by C_1. C_1-Fe. C_2. C_2-Fe clays.

Sorbent	Langmuir						Freundlich	
	Q_m	K_L	R_L	R^2	1/n	n	K_F	R^2
	(mg/g PO_4^{3-})	(L/mg)					(mg/g PO_4^{3-})(mg/L)$^{-1/n}$	
C_1	21.4	$1.84x10^{-03}$	0.23	0.97	0.7	1.4	0.1	0.92
C_1-Fe	38.0	$1.83x10^{-03}$	0.22	0.98	0.6	1.6	0.3	0.91
C_2	20.9	$9.81x10^{-03}$	0.06	0.97	0.8	1.3	0.1	0.92
C_2-Fe	37.6	$1.17x10^{-03}$	0.31	0.97	0.6	1.7	0.3	0.93

The phosphate adsorption process was governed by some physicochemical mechanisms including electrostatic attraction (physical adsorption) and complexation reaction (chemical adsorption). The adsorption capacities for clay minerals used for phosphate adsorption from aqueous solutions are reported in Table S3 of the supplementary section. The maximum adsorption capacities values reported using raw and synthetic iron-doped clays were between 10–40 mg/g P-PO_4^{3-}, which are comparable with the raw and iron-doped clays used in this study. Maximum adsorption capacity values up to 100 mg/ PO_4^{3-} were reported for phosphate removal using polymeric anion exchangers resins and fibber composites [45] [6] [3] The larger adsorption capacities, the mechanical strength and the operation flow-rates in column packed arrangement of polymeric exchangers involve an advantage in comparison with the iron-doped clays used in this study. [4] [17]. In addition, maximum adsorption capacity values up to 50 mg/g PO_4^{3-} were reported when using an iron (oxyhydr)oxides ferrihydrite impregnated polymeric exchangers [46]. However, from a practical and economical point of view, the potential use of such materials at full-scale is limited due to the large content od dissolved organic matter in solution. A convenient method to control the problem of particle size of iron hydroxides could be the preparation in a template such as clays, as it is proposed in this work.

3.4. Adsorption kinetic evaluation of the clay-based adsorbents

By plotting the phosphate adsorption capacity (Q_t) as a function of time, clay adsorbents (C_1, C_1-Fe, C_2 and C_2-Fe) extracted 50% of phosphate within 5 minutes of operation (Figure 4). The phosphate adsorption subsequently increased at a slower rate; reaching the equilibrium at approximately 10 minutes. The easy access of phosphate to the binding sites on surface of clays allowed fast adsorption due to their structure, as had been previously reported for open-pore mesoporous silica that reached equilibrium within 1 minute [47]. Otherwise, a mesoporous material (SBA-15) and its amino form (NH_2-SBA-15) reached the equilibrium above 110 min for metal ion removal. It seems the lowest passage to inner surface adsorbent promote lower adsorbent efficiency due to the reactivity of the bonding processes involved. Even though, NH_2-SBA-15 and SBA-15 have higher surface areas in comparison to the clays reported in this study [27]. Then, kinetic performance of iron-doped clays is very attractive for their application in stirred reactors.

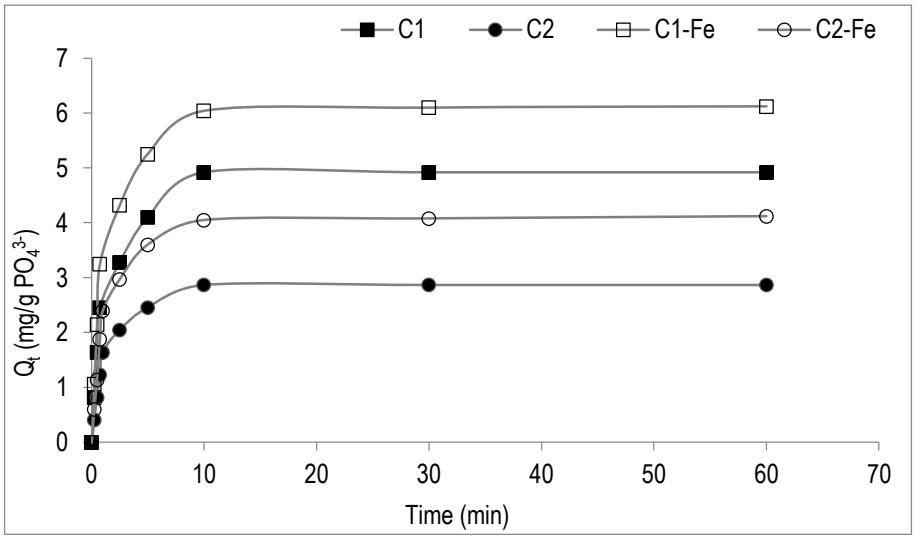

Figure 4 Kinetic of phosphate adsorption by C_1, C_1-Fe, C_2 and C_2-Fe clays (C_i: 100 mg/L PO_4^{3-}; V: 500 mL, w: 2.5 g and pH: 7).

The experimental data of phosphate adsorption on C_1, C_1-Fe, C_2 and C_2-Fe were adjusted to three conventional kinetic models (Table S1 of the supplementary section). The adsorption kinetic modelling explains the rate of phosphate adsorption from aqueous solution to a solid-phase interface at different conditions [43] (e.g., physisorption and chemisorption). Therefore, pseudo-

462 first and pseudo-second order kinetic models were used to explain the phosphate adsorption
463 mechanisms. The data were best fitted to the pseudo-second-order kinetic model with an R^2 value
464 ≈1. This fact supports the fact that phosphate was chemisorbed through monolayer adsorption as
465 previously described. Complexation reactions involving the iron oxyhydroxide species and
466 phosphate anions turns out to be the dominant phosphate adsorption mechanism in clay
467 adsorbents. Also, the experimental data demonstrated a good fitting to the intraparticular diffusion
468 kinetic model which describes the adsorbate diffusion-controlled in macroscopic adsorbent
469 particles.
470 In addition, kinetic parameters were obtained from the linear regression of the adsorption rate
471 equation of the Homogeneous Diffusion Model (HDM) and Shell Progressive Model (SPM) (Table
472 4). The analysis of the kinetic data of C_1, C_1-Fe, C_2 and C_2-Fe indicated that the adsorption
473 mechanisms governing the phosphate adsorption were well described by the HDM and SPM
474 according to the R^2 values closer to 1. The values of effective diffusion coefficients (D_p and D_f) were
475 in the range of 10^{-12} to 10^{-10} m^2/s, similar to other systems governed by chemisorption, as was
476 reported for a synthetic zeolite [48]. Two consecutive phases controlled the adsorption rate of
477 phosphate by raw and iron-doped clay adsorbents. There was an initial process of quick adsorption
478 of phosphate on the surface of the clay materials until saturation. Then, slower adsorption occurred,
479 and phosphate was diffused through the internal clay pores. This means quick phosphate removal
480 is due electrostatic attraction and the second stage of slow phosphate adsorption occurred by
481 complexation reactions. Thus, the mechanisms involved in phosphate removal determine the
482 kinetic efficiency of adsorbents. It is comparable to ligand exchange polymeric adsorbents where
483 the ligand coordinated to the central metal ion is after substituted by the phosphate anion. These
484 ligand exchangers develop slower kinetic performances than anion exchange and hydrogen
485 bonding adsorption mechanisms of conventional polymeric exchangers [4].

Table 4 Homogeneous Diffusion Model and Shell Progressive Model kinetic parameters obtained for phosphate uptake by C_1. C_1-Fe. C_2 and C_2-Fe clays.

	HDM						SPM			
Sorbent	D_f (m^2/s)	R^2	D_p (m^2/s)	R^2	K_F (m/s)	R^2	D_p (m^2/s)	R^2	k_s (m/s)	R^2
C_1	1.2E-10	0.95	8.1E-12	0.99	1.7E-06	0.79	1.8E-11	0.98	2.9E-08	0.90
C_1-Fe	2.8E-11	0.93	2.8E-12	0.96	7.9E-08	0.68	2.0E-10	0.93	3.3E-09	0.96
C_2	1.3E-10	0.94	9.4E-12	0.98	1.0E-06	0.72	2.2E-11	0.99	3.5E-08	0.97
C_2-Fe	5.4E-11	0.97	4.8E-12	0.98	1.4E-07	0.69	3.5E-12	0.97	5.6E-09	0.95

Kinetic parameters would be critical in the integration of the synthesised Fe-doped clays in stirred reactor-based applications. According to the kinetic parameters, even with low hydraulic residence times (e.g., shorter than 10 minutes), more than 90% of the adsorption equilibrium attainment would be reached. The performance of iron-doped clays was better than that obtained with natural zeolites in our previous studies where higher equilibrium times were obtained [49]. It is worth mentioning that kinetic depends on several parameters, such as the arrangement and the type of adsorbents used for phosphate removal. The fixed-bed column adsorption arrangement is conventionally limited for the iron-doped clay adsorbents used in this study. However, fixed-bed column is the best layout for phosphate removal at low levels where polymeric resins and fibbers adsorbents develop high efficiencies. The diffusion path of granular resin adsorbents is higher in comparison to fibrous adsorbents promoting low kinetic performances; where flow rate disturb their kinetic behaviour [17]. Therefore, kinetic efficiency of adsorbents is relevant when large volumes of treated water exist as is the case of urban wastewater and a rapid extraction is desired. Then, iron-doped clays can achieve these conditions for a rapid phosphate adsorption in low- and high-concentration feeds.

3.5. Effect of competitive anions typically present in treated wastewater

The phosphate adsorption capacity of clay adsorbents was determined when other ionic species were present in the solutions (Table 5a,b). The phosphate adsorption selectivity on C_1, C_1-Fe, C_2

and C_2-Fe was evaluated at equal level in comparison with main anions existing in urban wastewater. Adsorption changes were quantified in terms of the adsorption ratio (q^{mix}/q^0) on the presence of competing ions (q^{mix}) and in the absence of competing ions (q^0). At pH 7, both phosphate species ($H_2PO_4^-$ and HPO_4^{2-}) coexist in the solution. The phosphate adsorption capacity was reduced by sulphate, chloride and bicarbonate. The sulphate ion inhibited the adsorption of phosphate reporting a q^{mix}/q^0 ratio near to zero for all clay adsorbents. Sulphate has higher ionic charges and compete with phosphate through enhanced electrostatic interaction as has been reported for polymeric exchangers [6]. Therefore, the adsorption of phosphate at pH 7 (HPO_4^{2-}) was inhibited by sulphate ion according to the Helfferich's electroselectivity concept; in which the Donnan potential acts proportionally to the ionic charge [50]. Thus, the existence of equivalent content of sulphate limit the ability of phosphate (HPO_4^{2-}) to form hydrogen bonds at protonated sites of iron-doped clays [6]. The phosphate adsorption was also reduced by monovalent anions $Cl^- > HCO_3^-$. The less hydrated chloride anion was preferred in comparison to the highly hydrated phosphate. The results obtained for iron-doped clays is comparable with conventional anion exchange resins that prefer less hydrated anions to highly hydrated ones and exhibited the Hofmeister anion series behaviour [6] [37]. Moreover, a non-Hofmeister anion selectivity was provided by a crosslinked poly(allylamine) resin [51] and by a zirconium(IV) loaded fibrous used for phosphate removal [3]. Nevertheless, the nitrate ion potentiates the phosphate adsorption on clay adsorbents, obtaining a q^{mix}/q^0 ratio above 1. The increase of phosphate adsorption by the presence of nitrate was related to the Donnan invasion mechanism [52] [53]. A similar result was reported for a zirconium (IV) loaded fibrous adsorbent for phosphate removal in presence of sulphate. It can be explained in terms of the co-ion (sodium ion). When iron-doped clays adsorbed phosphate, it promotes an increase of sodium ion that enter in the exchanger phase through ion pair formation with phosphate maintaining electroneutrality. The increase of sodium ion concentration in aqueous solution promotes the equilibrium and enhanced the phosphate

adsorption [3]. The simultaneous existence of competing ions at the same concentration level decreased the phosphate adsorption on iron-doped clay adsorbents due to the competition for active sites. Otherwise, metal ligand exchange adsorbents are not strongly affected by common anions present in solution due to the phosphate outer sphere complex formation [54]. This suppose an advantage in comparison to the iron-doped clays used for phosphate adsorption used in this study, resulting in higher selectivity.

Table 5 Phosphate a) uptake capacity of C_1. C_1-Fe. C_2 and C_2-Fe in absence and presence of competing anions. and b) quantification in the terms of the sorption ratio (q^{mix}/q^0) on the presence of competing ions (q^{mix}) and in the absence of competing ions (q^0).

a)

Anions	Q_e (mg/g PO_4^{3-})			
	C_1	C_1-Fe	C_2	C_2-Fe
PO_4^{3-}	2.1±0.2	2.9±0.0	1.1± 0.1	1.7±0.0
PO_4^{3-} + NO_3^-	2.7±0.3	4.2±0.1	2.8±0.1	4.2±0.2
PO_4^{3-} +SO_4^{2-}	0.0±0.0	0.0±0.2	0.0±0.0	0.0±0.1
PO_4^{3-} + Cl^-	0.4±0.0	0.8±0.2	1.6±0.3	2.9±0.1
PO_4^{3-} + HCO_3^-	0.8±0.0	1.5±0.1	0.9±0.0	1.1±0.2
PO_4^{3-}+All anions	1.2±0.0	1.9±0.2	0.7±0.1	1.2±0.1

b)

Competing ion ratio	q^{mix}/q^0			
	C_1	C_1-Fe	C_2	C_2-Fe
	-	-	-	-
PO_4^{3-}+NO_3^-/PO_4^{3-}	1.3	1.5	2.5	2.4
PO_4^{3-}+SO_4^{2-}/PO_4^{3-}	0.0	0.0	0.0	0.0
PO_4^{3-}+ Cl^-/PO_4^{3-}	0.2	0.3	1.5	1.7

PO_4^{3-}+ HCO_3^-/PO_4^{3-}	0.4	0.5	0.8	1.1
PO_4^{3-}+All anions/PO_4^{3-}	0.6	0.7	0.6	0.7

3.6. Phosphate desorption studies simulating soil amendment applications

According to soil chemistry, soil pH can become acidic, basic or neutral; therefore, batch experiments were performed at different pH values (3.0, 6.0 and 10.0) using water as a regeneration solution. The phosphate desorption efficiencies of clay adsorbents onto raw and iron-doped clays were governed by physical and chemical adsorption, and it was not fully reversible (Figure 5). According to the results at pH 3 and 6, the monobasic anion phosphate specie ($H_2PO_4^-$) was the main specie recovered from adsorbents, since it is the main source of available phosphorus for plants [55]. The phosphate recovered at pH 6 from raw and doped clay adsorbents is higher for C_1 than C_2. This phosphate fraction was mainly physically adsorbed or linked by weak electrostatic bonds as was reported before when a neutral solution was used for phosphate desorption of natural modified zeolites [18]. At pH 10, the phosphate fraction recovered from clay adsorbents was limited even the hydroxide is a hardest Lewis base. The phosphate adsorption by the formation of chemical reactions (covalent bonds) to oxyhydroxide iron groups of clays could be partially reversed by strong basic solutions. In this condition, also the contents of phosphate anionic forms (e.g., $H_2PO_4^-$ and HPO_4^{2-}) were reduced. Phosphate exists mainly as triple charged anion, which partially avoids the formation of an inner sphere complex and has OH^- as a competing ion. In this work, a higher release of phosphate was reported using a desorption solution at acidic conditions for clay C_2. A difference was found in the regeneration solution at pH 3 between raw and iron-doped adsorbents clays since the phosphate released from C_2 and C_2-Fe was higher than that from C_1 and C_1-Fe. This effect can be attributed to the phosphate bonded to the alkaline earth elements. The C_1 and C_1-Fe contained higher amounts of Ca^{2+} and Mg^{2+} than the C_2 and C_2-Fe clays did. These elements impeded the release of loaded phosphate due to the inner sphere

surface complexes, electrostatic forces and surface precipitation mechanisms involved [56]. The higher phosphate desorption determined for C_2 and C_2-Fe could be explained in terms of the higher content of phosphate bonded to iron hydroxyl groups. At acidic conditions, it has been demonstrated that iron species complexed by surface hydroxyl groups of clays are desorbed [26]. Therefore, the phosphate bounded by iron hydroxyl groups is mainly released from clays at this condition. It should be noted that iron was not detected in the desorbed solutions. Therefore, iron was not released in comparison to the iron immobilized at the doping stage, determining the chemical stability of the iron-doped clays at the experimental conditions using at desorption stage. The reusability for long-term use of iron-doped clays is limited in comparison to other phosphate adsorbents such as polymeric exchangers and ligand exchangers [45]. Such materials can be used in several operational cycles without deterioration and maintaining their performance which balance their high cost of investment in a practical viewpoint [17]. Even if, the adsorbents used in this study seems to be inefficient for reuse, their low cost and availability brings new perspectives for final disposal. Since, the saturated phosphate iron-doped clays can be assigned for soil amendment applications such as saturated zeolites were used in our previous studies for plant growth [57].

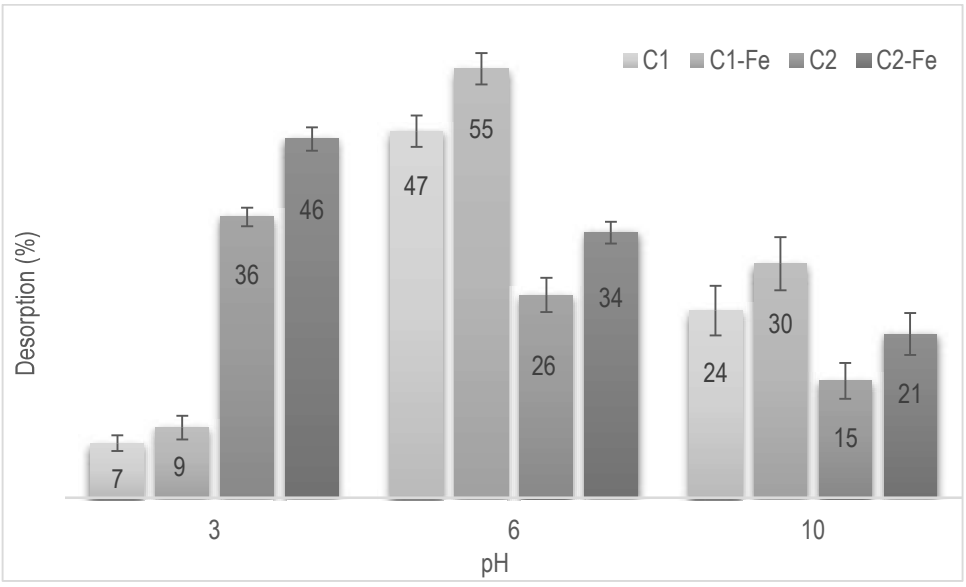

Figure 5 Phosphate desorption from C_1, C_1-Fe, C_2 and C_2-Fe clays at different pH conditions (V: 25 mL and w: 0.1 g).

3.7. Implications of the potential use of Fe-doped clays as low-cost adsorbents for phosphate recovery from WWTP

The P adsorption capacity shown by the synthesised Fe-doped clays from this study was compared with the values previously reported by inorganic adsorbents. P, N and blends of P and N containing loaded reactive adsorbents loaded with bio-solids from urban wastewater were proposed for sustainable soil enrichment, taking into account economic, agronomic and circularity criteria [58]. There are several examples of initiatives to promote valorisation pathways of nutrients from wastewater (Table S2, supplementary information).

Efforts to provide a feasibility analysis on the promotion of the P recovery and valorisation options using single-use low-cost adsorbents such as Fe-doped clays focused on economic and regulatory concerns are scarce. In the case of the EU, a new Directive on Fertilisers will be a useful tool that will promote and define the quality control of by-products to identify the type of agronomic application or potential applications in the solid amendment. In two previous studies with Al, Fe and Mn-doped natural zeolites the loaded carrier and the nutrient release rate with three different soils showed how the dissolution of soil minerals and soil acidity control the release of nutrients from the loaded carriers [16]. The proposed methodology on the development of low-cost sorbents is supported on the fact that natural clays are not containing trace of hazardous metals. Studies with natural zeolites demonstrated that enrichment due to the trace levels of hazardous metals in urban wastewater did not provide concerns on accumulation and latter release from the sorbent to the soil.

As can be seen in a large number of studies (Table S3, supplementary section, information online), increasing activity on the promotion of low-cost adsorption processes to recover P from wastewater. The general trend was the use of metal-hydroxide adsorbents (e.g., Al and Fe), as pure component or impregnated onto a high surface area adsorbent, typically of inorganic nature. However, some

examples on the use of organic adsorbents as polymeric macroporous supports (ion-exchangers of divinyl-benzene) have been also reported.

4. Conclusion

In this study, two raw clays were successfully doped with iron hydr(oxides) for the phosphate recovery from simulated urban treated wastewater is evaluated. The iron-doped clays can adsorb phosphate efficiently at neutral pH range which is an advantage in comparison with other adsorbents used with this purpose. The experimental data were best fitted to the Langmuir isotherm model and the intraparticular diffusion model. Phosphate adsorption was governed by the combined effect of physi-sorption and chemi-sorption. The occurrence of hydrogen bonding and complexation reactions were determined as the main mechanisms for phosphate adsorption to raw and doped clays. The presence of sulphate inhibited the phosphate adsorption limiting the ability of phosphate to form hydrogen bonds at protonated sites of iron-doped clays. The phosphate adsorption onto clays was also reduced by monovalent anions (chloride and bicarbonate) exhibited the Hofmeister anion series behaviour which is comparable with conventional polymeric anion exchangers. Finally, iron ions were not released during the phosphate adsorption and desorption stages revealing a good chemical stability of iron-doped clays. The reusability of iron-doped clays is limited in comparison to other phosphate adsorbents such as polymeric exchangers. However, saturated phosphate iron-doped clays can be used for soil amendment applications due to their low cost and availability. Since, natural minerals do not provide concerns on accumulation and latter release of hazardous contaminants from the adsorbent to the soil. Then, the use of iron-doped clays as single-use adsorbents could allow reaching the regulatory levels of total phosphorous in wastewater and being an alternative source of phosphorous.

Acknowledgements

This research was supported by the Waste2Product project (CTM2014-57302-R) and the R2MIT

643 project (CTM2017-85346-R) financed by the Ministerio de Economía y Competitividad (MINECO)
644 and the Catalan Government (Project Ref. 2017SGR312), Spain. Diana Guaya acknowledges the
645 financial support of Secretaría de Educación Superior, Ciencia, Tecnología e Innovación (Senescyt
646 - Ecuador) and Universidad Técnica Particular de Loja – Ecuador.

647 **5. References**

648 [1] F. Khan, A.A. Ansari, Eutrophication: an ecological vision, Bot. Rev. 71 (2005) 449–482.
649 [2] J. Álvarez, M. Roca, C. Valderrama, J.L. Cortina, A phosphorous flow analysis in Spain,
650 Sci. Total Environ. 612 (2018) 995–1006.
651 https://doi.org/https://doi.org/10.1016/j.scitotenv.2017.08.299.
652 [3] M.R. Awual, A. Jyo, T. Ihara, N. Seko, M. Tamada, K.T. Lim, Enhanced trace phosphate
653 removal from water by zirconium(IV) loaded fibrous adsorbent, Water Res. 45 (2011) 4592–
654 4600. https://doi.org/https://doi.org/10.1016/j.watres.2011.06.009.
655 [4] M.R. Awual, A. Jyo, S.A. El-Safty, M. Tamada, N. Seko, A weak-base fibrous anion
656 exchanger effective for rapid phosphate removal from water, J. Hazard. Mater. 188 (2011)
657 164–171. https://doi.org/https://doi.org/10.1016/j.jhazmat.2011.01.092.
658 [5] D.A. Almasri, N.B. Saleh, M.A. Atieh, G. McKay, S. Ahzi, Adsorption of phosphate on iron
659 oxide doped halloysite nanotubes, Sci. Rep. 9 (2019) 3232. https://doi.org/10.1038/s41598-
660 019-39035-2.
661 [6] M.R. Awual, A. Jyo, Assessing of phosphorus removal by polymeric anion exchangers,
662 Desalination. 281 (2011) 111–117. https://doi.org/10.1016/j.desal.2011.07.047.
663 [7] D. Guaya, C. Valderrama, A. Farran, C. Armijos, J.L. Cortina, Simultaneous phosphate and
664 ammonium removal from aqueous solution by a hydrated aluminum oxide modified natural
665 zeolite, Chem. Eng. J. 271 (2015) 204–213. https://doi.org/10.1016/j.cej.2015.03.003.
666 [8] L. Yuan, Z. Qiu, L. Yuan, M. Tariq, Y. Lu, J. Yang, Z. Li, S. Lyu, Adsorption and mechanistic
667 study for phosphate removal by magnetic Fe3O4-doped spent FCC catalysts adsorbent,

668 Chemosphere. 219 (2019) 183–190. https://doi.org/10.1016/j.chemosphere.2018.11.132.
669 [9] M. Hermassi, C. Valderrama, N. Moreno, O. Font, X. Querol, N.H. Batis, J.L. Cortina, Fly
670 ash as reactive sorbent for phosphate removal from treated waste water as a potential slow
671 release fertilizer, J. Environ. Chem. Eng. 5 (2017) 160–169.
672 https://doi.org/https://doi.org/10.1016/j.jece.2016.11.027.
673 [10] M. Zamparas, A. Gianni, P. Stathi, Y. Deligiannakis, I. Zacharias, Removal of phosphate
674 from natural waters using innovative modified bentonites, Appl. Clay Sci. 62–63 (2012) 101–
675 106. https://doi.org/10.1016/j.clay.2012.04.020.
676 [11] A.M. Awad, S.M.R. Shaikh, R. Jalab, M.H. Gulied, M.S. Nasser, A. Benamor, S. Adham,
677 Adsorption of organic pollutants by natural and modified clays: a comprehensive review,
678 Sep. Purif. Technol. 228 (2019) 115719.
679 https://doi.org/https://doi.org/10.1016/j.seppur.2019.115719.
680 [12] A.M. Alkafajy, T.M. Albayati, High performance of magnetic mesoporous modification for
681 loading and release of meloxicam in drug delivery implementation, Mater. Today Commun.
682 23 (2020) 100890. https://doi.org/https://doi.org/10.1016/j.mtcomm.2019.100890.
683 [13] G. Yuan, L. Wu, Allophane nanoclay for the removal of phosphorus in water and
684 wastewater, Sci. Technol. Adv. Mater. 8 (2007) 60–62.
685 https://doi.org/https://doi.org/10.1016/j.stam.2006.09.002.
686 [14] J. Bratby, Coagulation and flocculation in water and wastewater treatment, Third edit, IWA
687 Publishing, 2016.
688 [15] A.A. Zorpas, E. Kapetanios, G.A. Zorpas, P. Karlis, A. Vlyssides, I. Haralambous, M.
689 Loizidou, Compost produced from organic fraction of municipal solid waste, primary
690 stabilized sewage sludge and natural zeolite, J. Hazard. Mater. 77 (2000) 149–159.
691 https://doi.org/https://doi.org/10.1016/S0304-3894(00)00233-8.
692 [16] D. Guaya, C. Valderrama, A. Farran, T. Sauras, J.L. Cortina, Valorisation of N and P from

waste water by using natural reactive hybrid sorbents: nutrients (N,P,K) release evaluation in amended soils by dynamic experiments, Sci. Total Environ. 612 (2018). https://doi.org/10.1016/j.scitotenv.2017.08.248.

[17] M.R. Awual, M.A. Shenashen, A. Jyo, H. Shiwaku, T. Yaita, Preparing of novel fibrous ligand exchange adsorbent for rapid column-mode trace phosphate removal from water, J. Ind. Eng. Chem. 20 (2014) 2840–2847. https://doi.org/https://doi.org/10.1016/j.jiec.2013.11.016.

[18] D. Guaya, M. Hermassi, C. Valderrama, A. Farran, J.L. Cortina, Recovery of ammonium and phosphate from treated urban wastewater by using potassium clinoptilolite impregnated hydrated metal oxides as N-P-K fertilizer, J. Environ. Chem. Eng. 4 (2016) 3519–3526. https://doi.org/10.1016/j.jece.2016.07.031.

[19] M.H. McCrady. American Journal of Public Health and the Nations Health, Standard methods for the examination of water and wastewater (12th ed.), 2011.

[20] C. Valderrama, J.I. Barios, M. Caetano, A. Farran, J.L. Cortina, Kinetic evaluation of phenol/aniline mixtures adsorption from aqueous solutions onto activated carbon and hypercrosslinked polymeric resin (MN200), React. Funct. Polym. 70 (2010) 142–150. https://doi.org/https://doi.org/10.1016/j.reactfunctpolym.2009.11.003.

[21] G. Moussavi, S. Talebi, M. Farrokhi, R.M. Sabouti, The investigation of mechanism, kinetic and isotherm of ammonia and humic acid co-adsorption onto natural zeolite, Chem. Eng. J. 171 (2011) 1159–1169. https://doi.org/https://doi.org/10.1016/j.cej.2011.05.016.

[22] L. Mdlalose, M. Balogun, K. Setshedi, L. Chimuka, A. Chetty, Adsorption of phosphates using transition metals-modified bentonite clay, Sep. Sci. Technol. 54 (2019) 2397–2408. https://doi.org/10.1080/01496395.2018.1547315.

[23] J. Chang, J. Ma, Q. Ma, D. Zhang, N. Qiao, M. Hu, H. Ma, Adsorption of methylene blue onto Fe3O4/activated montmorillonite nanocomposite, Appl. Clay Sci. 119 (2016) 132–140.

https://doi.org/https://doi.org/10.1016/j.clay.2015.06.038.

[24] M.E.Z. Soulé, F. Barraqué, C.F. Morantes, F.M. Flores, M.A. Fernández, R.M.T. Sánchez, M.L. Montes, Magnetic nanocomposite based on montmorillonite, Fe oxides, and hydrothermal carbon: Synthesis, characterization and pollutants adsorption tests, Materialia. 15 (2021) 100973. https://doi.org/https://doi.org/10.1016/j.mtla.2020.100973.

[25] A.J. Fuller, S. Shaw, M.B. Ward, S.J. Haigh, J.F.W. Mosselmans, C.L. Peacock, S. Stackhouse, A.J. Dent, D. Trivedi, I.T. Burke, Caesium incorporation and retention in illite interlayers, Appl. Clay Sci. 108 (2015) 128–134. https://doi.org/https://doi.org/10.1016/j.clay.2015.02.008.

[26] T.B. Hofstetter, R.P. Schwarzenbach, S.B. Haderlein, Reactivity of Fe(II) species associated with clay minerals, Environ. Sci. Technol. 37 (2003) 519–528. https://doi.org/10.1021/es025955r.

[27] T. Albayati, A. Sabri, D. Abed, Adsorption of binary and multi heavy metals ions from aqueous solution by amine functionalized SBA-15 mesoporous adsorbent in a batch system, Desalin. WATER Treat. 151 (2019) 315–321. https://doi.org/10.5004/dwt.2019.23937.

[28] T. Albayati, Application of nanoporous material MCM-41 in a membrane adsorption reactor (MAR) as a hybrid process for removal of methyl orange, Desalin. WATER Treat. 151 (2019) 138–144. https://doi.org/10.5004/dwt.2019.23878.

[29] T.M. Albayati, A.A.A. Jassam, Synthesis and characterization of mesoporous materials as a carrier and release of prednisolone in drug delivery system, J. Drug Deliv. Sci. Technol. 53 (2019) 101176. https://doi.org/https://doi.org/10.1016/j.jddst.2019.101176.

[30] T. Ritschel, K.U. Totsche, Modeling the formation of soil microaggregates, Comput. Geosci. 127 (2019) 36–43. https://doi.org/https://doi.org/10.1016/j.cageo.2019.02.010.

[31] Y. Dehmani, A. Ed-Dra, O. Zennouhi, A. Bouymajane, F. Rhazi Filali, L. Nassiri, S.

Abouarnadasse, Chemical characterization and adsorption of oil mill wastewater on Moroccan clay in order to be used in the agricultural field, Heliyon. 6 (2020) e03164. https://doi.org/https://doi.org/10.1016/j.heliyon.2020.e03164.

[32] S. Barakan, V. Aghazadeh, Synthesis and characterization of hierarchical porous clay heterostructure from Al, Fe -pillared nano-bentonite using microwave and ultrasonic techniques, Microporous Mesoporous Mater. 278 (2019) 138–148. https://doi.org/https://doi.org/10.1016/j.micromeso.2018.11.031.

[33] R. Mukhopadhyay, K.M. Manjaiah, S.C. Datta, R.K. Yadav, B. Sarkar, Inorganically modified clay minerals: preparation, characterization, and arsenic adsorption in contaminated water and soil, Appl. Clay Sci. 147 (2017) 1–10. https://doi.org/https://doi.org/10.1016/j.clay.2017.07.017.

[34] A. Ahmed, Y. Chaker, E.H. Belarbi, O. Abbas, J.N. Chotard, H.B. Abassi, A.N. Van Nhien, M. El Hadri, S. Bresson, XRD and ATR/FTIR investigations of various montmorillonite clays modified by monocationic and dicationic imidazolium ionic liquids, J. Mol. Struct. 1173 (2018) 653–664. https://doi.org/https://doi.org/10.1016/j.molstruc.2018.07.039.

[35] J. Lŭ, H. Liu, R. Liu, X. Zhao, L. Sun, J. Qu, Adsorptive removal of phosphate by a nanostructured Fe–Al–Mn trimetal oxide adsorbent, Powder Technol. 233 (2013) 146–154. https://doi.org/10.1016/j.powtec.2012.08.024.

[36] M. Kosmulski, The pH dependent surface charging and points of zero charge. VII. Update, Adv. Colloid Interface Sci. 251 (2018) 115–138. https://doi.org/https://doi.org/10.1016/j.cis.2017.10.005.

[37] M.R. Awual, M.M. Hasan, A.M. Asiri, M.M. Rahman, Cleaning the arsenic(V) contaminated water for safe-guarding the public health using novel composite material, Compos. Part B Eng. 171 (2019) 294–301. https://doi.org/https://doi.org/10.1016/j.compositesb.2019.05.078.

768 [38] M.R. Awual, Efficient phosphate removal from water for controlling eutrophication using
769 novel composite adsorbent, J. Clean. Prod. 228 (2019) 1311–1319.
770 https://doi.org/https://doi.org/10.1016/j.jclepro.2019.04.325.
771 [39] M.R. Awual, T. Yaita, S. Suzuki, H. Shiwaku, Ultimate selenium(IV) monitoring and removal
772 from water using a new class of organic ligand based composite adsorbent, J. Hazard.
773 Mater. 291 (2015) 111–119. https://doi.org/https://doi.org/10.1016/j.jhazmat.2015.02.066.
774 [40] D. Guaya, C. Valderrama, A. Farran, J.L. Cortina, Modification of a natural zeolite with
775 Fe(III) for simultaneous phosphate and ammonium removal from aqueous solutions, J.
776 Chem. Technol. Biotechnol. 91 (2016) 1737–1746. https://doi.org/10.1002/jctb.4763.
777 [41] M.R. Awual, M.M. Hasan, M.A. Khaleque, Efficient selenium(IV) detection and removal from
778 water by tailor-made novel conjugate adsorbent, Sensors Actuators B Chem. 209 (2015)
779 194–202. https://doi.org/https://doi.org/10.1016/j.snb.2014.11.010.
780 [42] T. Albayati, A. Sabri, D. Abed, Functionalized SBA-15 by amine group for removal of Ni(II)
781 heavy metal ion in the batch adsorption system, Desalin. WATER Treat. 174 (2020) 301–
782 310. https://doi.org/10.5004/dwt.2020.24845.
783 [43] S.T. Kadhum, G.Y. Alkindi, T.M. Albayati, Eco friendly adsorbents for removal of phenol
784 from aqueous solution employing nanoparticle zero-valent iron synthesized from modified
785 green tea bio-waste and supported on silty clay, Chinese J. Chem. Eng. (2020).
786 https://doi.org/https://doi.org/10.1016/j.cjche.2020.07.031.
787 [44] L.G. Yan, Y.Y. Xu, H.Q. Yu, X.D. Xin, Q. Wei, B. Du, Adsorption of phosphate from aqueous
788 solution by hydroxy-aluminum, hydroxy-iron and hydroxy-iron-aluminum pillared bentonites,
789 J. Hazard. Mater. 179 (2010) 244–250. https://doi.org/10.1016/j.jhazmat.2010.02.086.
790 [45] M.R. Awual, S.A. El-Safty, A. Jyo, Removal of trace arsenic(V) and phosphate from water
791 by a highly selective ligand exchange adsorbent, J. Environ. Sci. 23 (2011) 1947–1954.
792 https://doi.org/https://doi.org/10.1016/S1001-0742(10)60645-6.

793 [46] G. Zelmanov, R. Semiat, The influence of competitive inorganic ions on phosphate removal
794 from water by adsorption on iron (Fe+3) oxide/hydroxide nanoparticles-based
795 agglomerates, J. Water Process Eng. 5 (2015) 143–152.
796 https://doi.org/https://doi.org/10.1016/j.jwpe.2014.06.008.
797 [47] W. Chouyyok, R.J. Wiacek, K. Pattamakomsan, T. Sangvanich, R.M. Grudzien, G.E.
798 Fryxell, W. Yantasee, Phosphate removal by anion binding on functionalized nanoporous
799 sorbents., Environ. Sci. Technol. 44 (2010) 3073–3078.
800 https://doi.org/10.1021/es100787m.Phosphate.
801 [48] M.S. Onyango, D. Kuchar, M. Kubota, H. Matsuda, Adsorptive removal of phosphate ions
802 from aqueous solution using synthetic zeolite, Ind. Eng. Chem. Res. 46 (2007) 894–900.
803 https://doi.org/10.1021/ie060742m.
804 [49] D. Guaya, C. Valderrama, A. Farran, J.L. Cortina, Simultaneous nutrients (N,P) removal by
805 using a hybrid inorganic sorbent impregnated with hydrated manganese oxide, J. Environ.
806 Chem. Eng. 5 (2017) 1516–1525. https://doi.org/10.1016/j.jece.2017.02.030.
807 [50] F. Helfferich, Ion exchange, McGraw-Hill, New York, NY, 1995.
808 [51] M.R. Awual, A. Jyo, Rapid column-mode removal of arsenate from water by crosslinked
809 poly(allylamine) resin, Water Res. 43 (2009) 1229–1236.
810 https://doi.org/https://doi.org/10.1016/j.watres.2008.12.018.
811 [52] F.G. Donnan, Theory of membrane equilibria and membrane potentials in the presence of
812 non-dialysing electrolytes. A contribution to physical-chemical physiology, J. Memb. Sci.
813 100 (1995) 45–55. https://doi.org/https://doi.org/10.1016/0376-7388(94)00297-C.
814 [53] F. Helfferich, Ion Exchange, McGraw-Hill, New York, NY, 1962.
815 [54] M.R. Awual, A. Jyo, Assessing of phosphorus removal by polymeric anion exchangers,
816 Desalination. 281 (2011) 111–117. https://doi.org/10.1016/j.desal.2011.07.047.
817 [55] A. Moreno Reséndez, Elementos nutritivos: asimiliacion, funciones, toxicidad e

indisponibilidad en los suelos, LibrosEnRed, 2007.

[56] M. Talebi Atouei, R. Rahnemaie, E. Goli Kalanpa, M.H. Davoodi, Competitive adsorption of magnesium and calcium with phosphate at the goethite water interface: kinetics, equilibrium and CD-MUSIC modeling, Chem. Geol. 437 (2016) 19–29. https://doi.org/https://doi.org/10.1016/j.chemgeo.2016.05.004.

[57] D. Guaya, A. Mendoza, C. Valderrama, A. Farran, T. Sauras-Yera, J.L. Cortina, Use of nutrient-enriched zeolite (NEZ) from urban wastewaters in amended soils: Evaluation of plant availability of mineral elements, Sci. Total Environ. 727 (2020) 138646. https://doi.org/https://doi.org/10.1016/j.scitotenv.2020.138646.

[58] D. Cordell, A. Rosemarin, J.J. Schröder, A.L. Smit, Towards global phosphorus security: a systems framework for phosphorus recovery and reuse options, Chemosphere. 84 (2011) 747–758. https://doi.org/https://doi.org/10.1016/j.chemosphere.2011.02.032.